metals

MDPI

Article

Influence of 0.5% Ag Addition on Low-Cycle Fatigue Behavior of Hot-Extruded Al-5Cu-0.8Mg-0.15Zr-0.2Sc Alloy Subjected to Peak-Aging Treatment

Ying Wang [1,2], Lijia Chen [1,2,*], Ge Zhou [1,2], Ruochong Liu [1,2] and Siqian Zhang [1,2]

[1] School of Materials Science and Engineering, Shenyang University of Technology, Shenyang 110870, China; 15140066981@163.com (Y.W.); zhouge@sut.edu.cn (G.Z.); lrclyric96@163.com (R.L.); sqzhang@alum.imr.ac.cn (S.Z.)

[2] Shenyang Key Laboratory of Advanced Structural Materials and Applications, Shenyang University of Technology, Shenyang 110870, China

* Correspondence: chenlijia@sut.edu.cn

Abstract: The total strain amplitude controlled low-cycle fatigue tests were performed at room temperature and 200 °C to clarify the influence of 0.5% Ag addition on the low-cycle fatigue behavior of an Al-5Cu-0.8Mg-0.15Zr-0.2Sc (in wt.%) alloy subjected to the peak-aging treatment after hot extrusion and solid solution treatment. The experimental results demonstrate that during low-cycle fatigue deformation, peak-aged Al-5Cu-0.8Mg-0.15Zr-0.2Sc(-0.5Ag) alloys exhibit cyclic hardening, cyclic stability, or cyclic hardening followed by cyclic stability, depending on the Ag addition, imposed total strain amplitude, and testing temperature. The addition of 0.5% Ag greatly increases the low-cycle fatigue life of peak-aged Al-5Cu-0.8Mg-0.15Zr-0.2Sc alloy, where the maximum rising amplitude is about 126.7% at ambient temperature and approximately 90.1% at 200 °C. Furthermore, it has been discovered that the addition of 0.5% Ag has no effect on the beginning and spreading modes of low-cycle fatigue fractures. For the peak-aged Al-5Cu-0.8Mg-0.15Zr-0.2Sc(-0.5Ag) alloys subjected to low-cycle fatigue deformation at different total strain amplitudes and testing temperatures used in this investigation, fatigue cracks initiate trans granularly at the free surface of the fatigue specimen and propagate in a trans granular mode.

Keywords: Al-Cu-Mg alloy; hot extrusion; low-cycle fatigue; aging treatment; fatigue life

Citation: Wang, Y.; Chen, L.; Zhou, G.; Liu, R.; Zhang, S. Influence of 0.5% Ag Addition on Low-Cycle Fatigue Behavior of Hot-Extruded Al-5Cu-0.8Mg-0.15Zr-0.2Sc Alloy Subjected to Peak-Aging Treatment. *Metals* **2023**, *13*, 1734. https://doi.org/10.3390/met13101734

Academic Editors: Giovanni Meneghetti and Lakhdar Taleb

Received: 16 August 2023
Revised: 22 September 2023
Accepted: 10 October 2023
Published: 12 October 2023

1. Introduction

Due to their high specific strength, excellent heating resistance, and technical performance, aluminum alloys of the Al-Cu-Mg series have been extensively utilized in the aerospace industry. It has been well established that a small Zr and Sc addition to the Al-Cu-Mg series aluminum alloys can increase strength and ductility while also raising the recrystallization temperature. The phenomenon is caused by the creation of very tiny $Al(Sc, Zr)_3$ particles, which function as grain boundary pinners and microstructure stabilizers [1–3]. It was also discovered that adding Sc to an extruded Al-Cu-Mg-Ag-Zr base alloy from room temperature to 300 °C accelerates the aging hardening process and improves the maximum hardness and yield strength [4].

The Al-Cu-Mg series alloys have undergone this microalloying process, which has proven to be effective in improving the mechanical properties of wrought Al alloys, particularly those at high temperatures [5–9]. For instance, a homogeneous distribution of coexisting θ′ and Ω precipitates on the matrix (001) and (111) planes, respectively, might enhance the Al-8Cu-0.5Mg-(Mg, Ti, Zr) alloy with the addition of 0.6% Ag, but the alloy without Ag could only be strengthened by the θ′ precipitate. As a result, especially at the higher temperature, the alloy containing Ag showed significantly enhanced ultimate tensile strength and yield strength [10]. Al-Cu-Mg-Ag alloys with Ag contents ranging

from 0.14 to 0.57 wt% had been noted [11], The Ag concentration was raised to hasten the aging hardening response at 165 °C. The alloy containing 0.14% Ag had the lowest hardening response, whereas the alloy containing 0.57% Ag showed the maximum hardening response. According to studies on the impact of Ag content on the mechanical characteristics and thermal stability of Al-Cu-Mg-Ag alloys [12], both tensile strength and ultimate endurance strength significantly enhanced with raising the Ag percentage. The increase in alloy strength is directly related to the fact that increasing the Ag concentration encouraged the nucleation of the Ω precipitate as the predominant strengthening phase and that the Ω phase did not coarsen after long-term endurance. Wang et al. [13] investigated the effect of non-isothermal aging treatment on the precipitation behavior and mechanical properties of the Al-Cu-Mg-Ag alloy, and found that the heating aging treatment could modify the size and density of the Ω phase, thereby enhancing the mechanical properties of the alloy.

In the investigation on the low-cycle fatigue behavior performed by Gazizov and Kaibyshev for an Al-Cu-Mg-Ag alloy with T6 and T840 states, it had been revealed that at the total strain amplitudes higher than 0.55%, the initial weak hardening occurred and an insignificant softening was followed [14]. The research results from Gazizov and Kaibyshev indicated that the fatigue lifetimes of the Al-Cu-Mg-Ag alloy with T6 and T840 states were nearly equal under the high-cycle fatigue loading condition, since the effect of thermomechanical processing on the initiation and growth mechanisms of fatigue crack was minimal [15]. According to the research on the three-point bending fatigue behavior of Al-Cu-Mg-Ag alloys with different Mg contents, Wang et al. [16] noted that the 0.70 wt.% Mg alloy had a higher fatigue performance than the 1.15 wt.% Mg alloy, where the fatigue life was primarily correlated with the density of constituent particles. The investigation of Burba et al. [17] on the fatigue properties of an Al-Cu-Mg-Ag alloy subjected to the peak aged (T6) and peak-aged interrupted (T6I4) treatments was reported that there was almost no difference in the mean lifetime for either heat treatment, but there was a significant difference in the minimum lifetimes, where the peak-aged condition displayed a higher propensity for the life-limiting failure mechanisms. According to the research from Bai et al. [18], for an Al-Cu-Mg-Ag alloy with a low Cu/Mg ratio, the initial light artificial aging was found to improve the alloy's resistance to fatigue crack propagation, whereas long-term aging at 150 °C after initial aging treatments was found to significantly worsen the alloy's resistance to fatigue crack propagation. According to the research from Duan et al. [19], the presence of Cu-Mg clusters in the matrix gave the Al-Cu-Mg-Ag alloy with a Cu/Mg ratio close to 4 and aging treatment at 165 °C for 30 min. the best resistance to fatigue crack formation. In the study of the crack resistance of an Al-Cu-Mg-Ag alloy with a high doping element content, Zhemchuzhnikova et al. [20] found that the alloy had a high stress intensity factor threshold value for the initiation of fatigue cracks, whereas the nonuniform distribution of second-phase particles decreased the crack resistance. According to the research carried out by Bai et al. [21], the presence of crystallographic secondary cracks could greatly increase the fatigue fracture propagation resistance when rare earth Er is added to an Al-Cu-Mg-Ag alloy. When Lumley et al. [22] compared the effects of underaging and peak-aging on the fatigue behavior of an Al-Cu-Mg-Ag alloy, they discovered that underaging increased the alloy's resistance to fatigue cracking. Hu et al. [23] found that the high intensity P-texture sheet had a lower fatigue crack propagation rate and a higher damage tolerance than the random texture sheet based on research on the influence of P-texture on the fatigue crack propagation resistance of an Al-Cu-Mg-Ag alloy. Although some studies have been performed on the fatigue behavior of Al-Cu-Mg-Ag alloys, there have not been many studies performed on how adding Ag affects the fatigue behavior of the Al-Cu-Mg series alloys.

In this study, a heat-resistant aluminum alloy was created by adding alloying elements like Zr, Sc, and Ag to the Al-5Cu-0.8Mg series alloy. The low-cycle fatigue behaviors of the alloys at room temperature and 200 °C were explored by conducting low-cycle fatigue experiments on the extruded Al-5Cu-0.8Mg-0.15Zr-0.2Sc(-0.5Ag) alloys. In order to clarify the low-cycle fatigue deformation and fracture behaviors of the 0.5%Ag containing Al-Cu-

Mg series heat-resistant alloys and to provide the reliable reference for the engineering application of Al-5Cu-0.8Mg-0.15Zr-0.2Sc(-0.5Ag) alloys, the influence rule of the Ag element on the low-cycle fatigue behavior of the alloy at both room temperature and elevated temperatures was also determined.

2. Experimental Procedures

Cast-ingot metallurgy was utilized to produce the Al-5Cu-0.8Mg-0.15Zr-0.2Sc(-0.5Ag) alloys cast ingots (wt.%) using industrially pure Al, Mg, and Ag, as well as intermediate alloys of Al-Cu, Al-Sc, and Al-Zr. The cast ingots were first homogenized at 500 °C for 24 h before being extruded at 430 °C into 20 mm diameter bars. The bars were subjected to solid solution and aging treatments in a resistance furnace of the SX-4-10-box design. After two hours of solution treatment at 510 °C, the temperature was cooled with water. After the aging treatment at 180 °C for 2 to 10 h, air cooling was applied. The low-cycle fatigue specimen with the gauge diameter of 8 mm and gauge length of 14 mm was fabricated from the peak-aged Al-5Cu-0.8Mg-0.2Sc-0.15Zr(-0.5Ag) alloy bars. An MTS Landmark 370.10 servo-hydraulic fatigue testing machine was used to conduct the low-cycle fatigue tests in an air-conditioned environment. The testing temperatures were room temperature and 200 °C. The adopted cyclic waveform was the sinusoidal wave, and 0.5 Hz was chosen as the cycle frequency. The strain ratio was -1 because the entire fully-reversed tension and compression loading mode was controlled by the overall strain amplitude. The low-cycle fatigue tests were run until the cyclic stress amplitude dropped to a 75% value, approximately, of peak stress amplitude attained in whole cyclic deformation process. Additionally, the low-cycle fatigue life was determined to equal the corresponding amount of cycles.

The fracture surface topography of the fatigue specimens was observed and analyzed using an S-3400N scanning electron microscope (SEM). The microstructure of the alloy in the fatigue deformation zone was characterized using a JEM-2100 transmission electron microscope (TEM). The TEM samples were produced by a Struers TenuPol-5 twin-jet electropolishing apparatus. The adopted electrolytic solution was 30%HNO_3 + 70%CH_3OH solution, the temperature of the electrolytic solution was controlled around −30 °C, and the voltage was 21 V.

3. Experimental Results

3.1. Cyclic Stress Response

The cyclic stress response curve, which displays the cyclic stress amplitude versus the number of cycles, can be used to illustrate a material's cyclic stress response behavior under low-cycle fatigue loading. Cyclic hardening or cyclic softening occurs when the cyclic stress amplitude increases or decreases as the number of cycles increases. Cyclic stability occurs when the cyclic stress amplitude remains essentially constant as the number of cycles increases. The inclusion of alloying elements can either enhance or inhibit the development of cyclic hardening, depending on the type and amount of alloying element added. Figure 1 displays the cyclic stress response curves for the peak-aged Al-5Cu-0.8Mg-0.15Zr-0.2Sc(-0.5Ag) alloys at room temperature (RT) and various total strain amplitudes. Figure 1a–d reveal that the peak-aged Al-5Cu-0.8Mg-0.15Zr-0.2Sc alloy initially exhibits an increase trend as the number of cycles increases; however, then, basically remains constant after reaching a certain number of cycles. Total strain amplitudes range from 0.3% to 0.8%. This indicates that the alloy responds to stress by cycling between cyclic hardening and cyclic stability at total strain amplitudes between 0.3% and 0.8%. However, as demonstrated in Figure 1e, only the cyclic hardening can be seen at the high total strain amplitude of 1.0%. A steady cyclic stress response behavior can be observed for the peak-aged Al-5Cu-0.8Mg-0.15Zr-0.2Sc-0.5Ag alloy when it is subjected to low-cycle fatigue deformation at total strain amplitudes of 0.3 and 0.4%, as shown in Figure 1a,b. The peak-aged Al-5Cu-0.8Mg-0.15Zr-0.2Sc-0.5Ag alloy first displays cyclic hardening for a limited number of cycles before exhibiting cyclic stability, as illustrated in Figure 1c, when the imposed total strain

amplitude is 0.6%. The peak-aged Al-5Cu-0.8Mg-0.15Zr-0.2Sc-0.5Ag alloy experiences cyclic hardening during entire fatigue deformation at total strain amplitudes of 0.8% and 1.0%, as shown in Figure 1d,e. Additionally, as can be seen from Figure 1, although there is a difference in the cyclic stress response behavior of the alloys with and without the Ag addition, the cyclic stress amplitude of the peak-aged Al-5Cu-0.8Mg-0.15Zr-0.2Sc-0.5Ag alloy is higher than that of the peak-aged Al-5Cu-0.8Mg-0.15Zr-0.2Sc alloy at each total strain amplitude used in this investigation. The difference in the cycle stress amplitude between the two alloys is significantly greater in the early stages of fatigue deformation but becomes much smaller as fatigue progresses. The imposed stress required for the tensile and compressive deformation at each cycle is often substantially higher; and, as a result, the corresponding cyclic deformation resistance is higher, as is the case with greater cyclic stress amplitudes. The previously mentioned fact suggests that under low-cycle fatigue loading conditions at room temperature, the peak-aged Al-5Cu-0.8Mg-0.15Zr-0.2Sc-0.5Ag alloy has higher cyclic deformation resistance than the peak-aged Al-5Cu-0.8Mg-0.2Sc alloy.

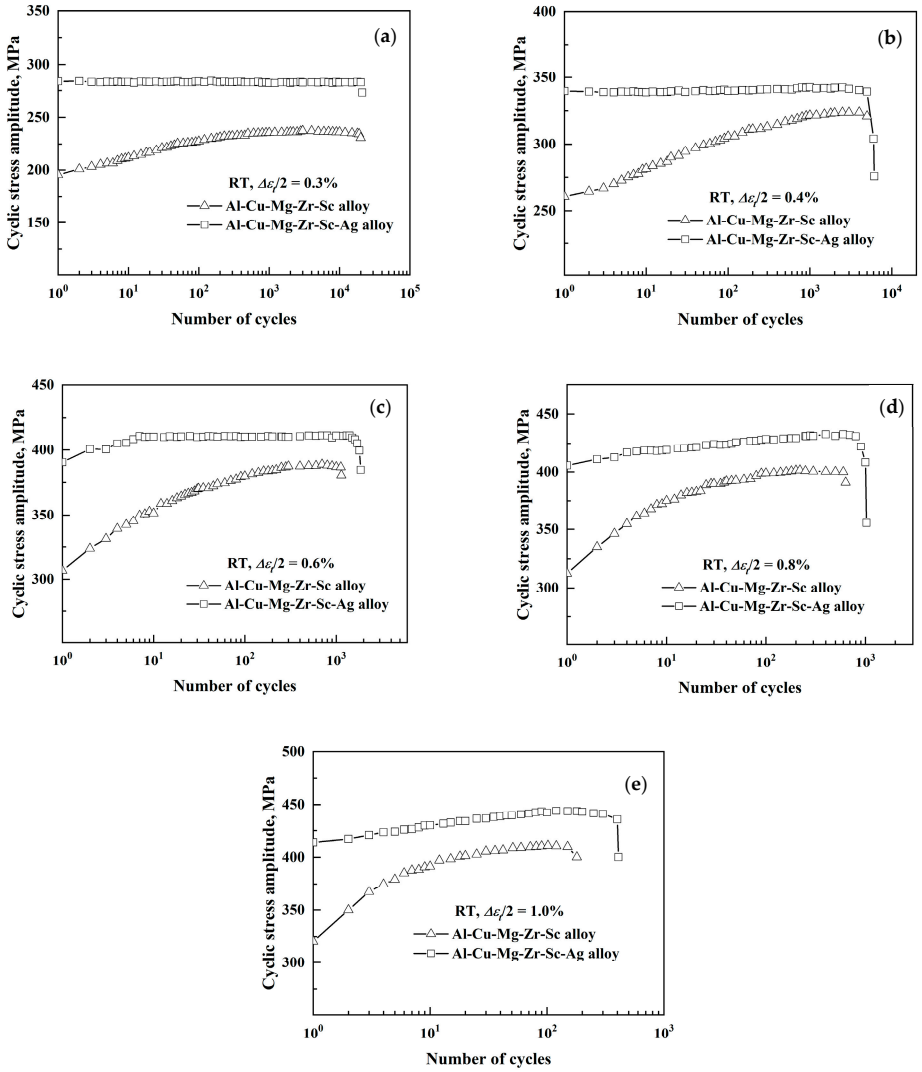

Figure 1. Cyclic stress response curves of peak-aged Al-5Cu-0.8Mg-0.15Zr-0.2Sc(-0.5Ag) alloys at room temperature and various total strain amplitudes: (**a**) 0.3%, (**b**) 0.4%, (**c**) 0.6%, (**d**) 0.8%, (**e**) 1.0%.

Figure 2 shows the cyclic stress response curves at 200 °C and various total strain amplitudes for peak-aged Al-5Cu-0.8Mg-0.15Zr-0.2Sc(-0.5Ag) alloys. The Al-5Cu-0.8Mg-0.15Zr-0.2Sc alloy exhibits cyclic hardening in the earlier stage of fatigue deformation and stable cyclic stress response behavior in the later stage of fatigue deformation, as shown

in Figure 2a,b, respectively, when total strain amplitudes of 0.3% and 0.4% are imposed. The cyclic hardening behavior can be observed during the entire cycle deformation of the Al-5Cu-0.8Mg-0.15Zr-0.2Sc at higher total strain amplitudes ranging from 0.5% to 0.7%, as shown in Figure 2c–e. For the peak-aged Al-5Cu-0.8Mg-0.15Zr-0.2Sc-0.5Ag alloy, steady cyclic stress response occurs throughout the fatigue deformation, as shown in Figure 2a–c, when the high temperature low-cycle fatigue deformation is carried out at total strain amplitudes of 0.3% to 0.5%. The Al-5Cu-0.8Mg-0.15Zr-0.2Sc-0.5Ag alloy demonstrates the cyclic hardening in the entire fatigue deformation process at the total strain amplitudes of 0.6% and 0.7%, as shown in Figure 2d,e. Additionally, it can be noted that the peak-aged Al-5Cu-0.8Mg-0.15Zr-0.2Sc-0.5Ag alloy exhibits a much greater cyclic stress amplitude than the peak-aged Al-5Cu-0.8Mg-0.15Zr-0.2Sc alloy in the early stage of high temperature low-cycle fatigue deformation. The cyclic stress amplitudes of peak-aged Al-5Cu-0.8Mg-0.15Zr-0.2Sc-0.5Ag alloy at various total strain amplitudes, except for that at the total strain amplitude of 0.5%, are a bit higher than those of the peak-aged Al-5Cu-0.8Mg-0.15Zr-0.2Sc alloy during the later stages of fatigue deformation. This indicates that the peak-aged Al-5Cu-0.8Mg-0.15Zr-0.2Sc-0.5Ag alloy, likewise, provides stronger cycle deformation resistance than the peak-aged Al-5Cu-0.8Mg-0.15Zr-0.2Sc alloy at the testing temperature of 200 °C.

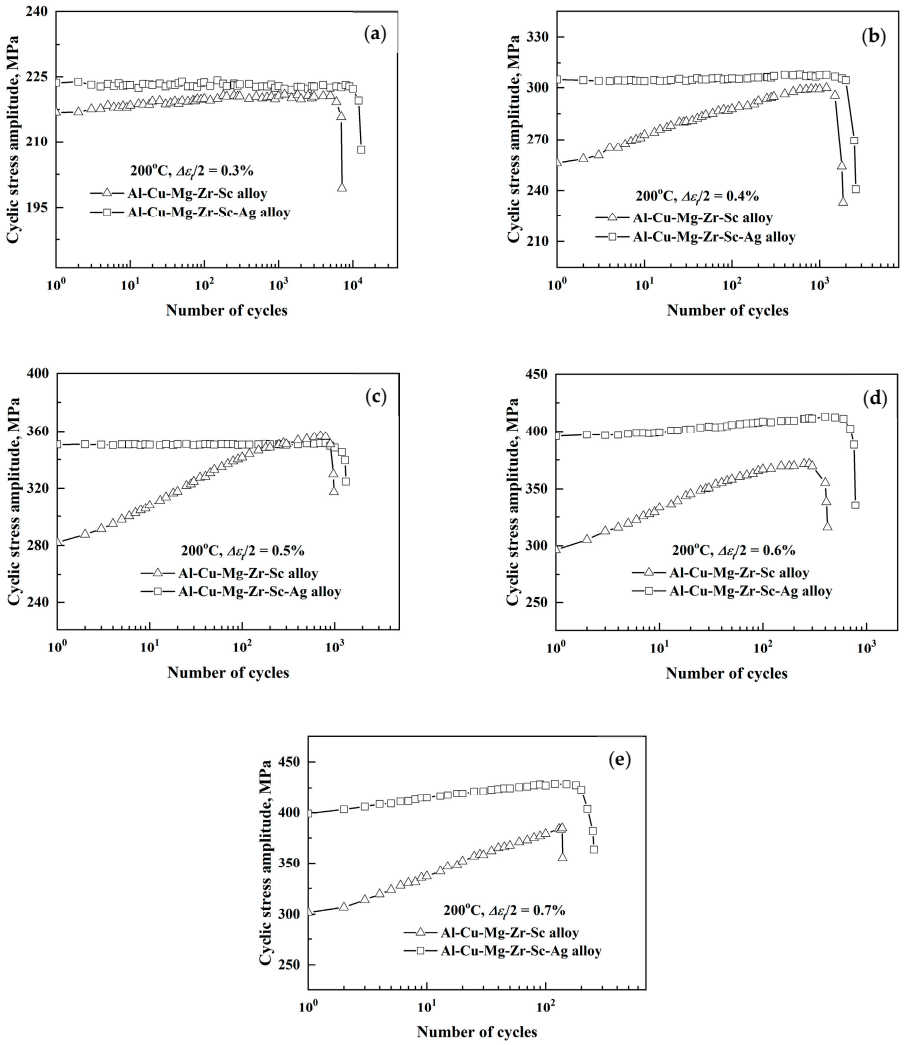

Figure 2. Cyclic stress response curves of peak-aged Al-5Cu-0.8Mg-0.15Zr-0.2Sc(-0.5Ag) alloys at 200 °C and various total strain amplitudes: (**a**) 0.3%, (**b**) 0.4%, (**c**) 0.5%, (**d**) 0.6%, (**e**) 0.7%.

3.2. Fatigue Life

For the peak-aged Al-5Cu-0.8Mg-0.15Zr-0.2Sc(-0.5Ag) alloys, Figure 3 shows the imposed total strain amplitudes against fatigue life curves under the low-cycle fatigue loading condition at both room temperature and 200 °C. As seen in Figure 3a, the fatigue life of the Al-5Cu-0.8Mg-0.15Zr-0.2Sc-0.5Ag alloy at room temperature is greater than that of the Al-5Cu-0.8Mg-0.15Zr-0.2Sc alloy for total strain amplitudes ranging from 0.3% to 1.0%. Although the difference in the low-cycle fatigue life is considerably smaller at the total strain amplitude of 0.3% for two Al-5Cu-0.8Mg-0.15Zr-0.2Sc alloys with and without the addition of Ag, the corresponding maximum extending amplitude is around 126.7% at ambient temperature. The fatigue life of peak-aged Al-5Cu-0.8Mg-0.15Zr-0.2Sc-0.5Ag alloy under various total strain amplitudes used in this investigation is significantly longer than one of Al-5Cu-0.8Mg-0.15Zr-0.2Sc alloy, where the increasing amplitude in the fatigue life is about 90.1%, as shown in Figure 3b when the low-cycle fatigue deformation is carried out at 200 °C. It indicates that peak-aged Al-5Cu-0.8Mg-0.15Zr-0.2Sc alloy at both room temperature and 200 °C can have its low-cycle fatigue life extended by the addition of 0.5% Ag.

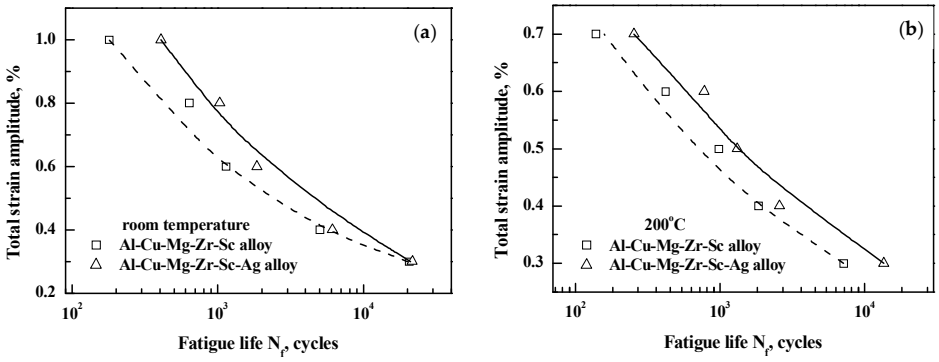

Figure 3. Total strain amplitude versus fatigue life curves of peak-aged Al-5Cu-0.8Mg-0.15Zr-0.2Sc(-0.5Ag) alloys at different testing temperatures: (**a**) room temperature, (**b**) 200 °C.

In actuality, the total strain amplitude ($\Delta\varepsilon_t/2$) for the total strain amplitude regulated low-cycle fatigue deformation is made up of the plastic strain amplitude ($\Delta\varepsilon_t/2$) and elastic strain amplitude ($\Delta\varepsilon_t/2$). Cycle plastic strain will cause fatigue damaging, which will affect the fatigue life and cycle deformation resistance. In general, the empirical equation linking the plastic strain amplitude and low-cycle fatigue life (N_f) can be written as

$$\Delta\varepsilon_p/2 = \varepsilon'_f(2N_f)^c \quad (1)$$

where $2N_f$ represents the number of reversals to failure, ε'_f is the fatigue ductility coefficient, and c is the fatigue ductility exponent.

On the other hand, the relation between the low-cycle fatigue and the elastic strain amplitude can be expressed as

$$\Delta\varepsilon_e/2 = \frac{\sigma'_f}{E}(2N_f)^b \quad (2)$$

where E is the Young's modulus, σ'_f is the fatigue strength coefficient, and b is the fatigue strength exponent.

Figure 4 depicts the plastic strain amplitude and elastic strain amplitude vs. reversals to failure curves of peak-aged Al-5Cu-0.8Mg-0.15Zr-0.2Sc(-0.5Ag) alloys at room temperature and 200 °C. The strain amplitude data in Figure 4 were obtained from the half-life hysteresis loop depicted in Figure 5. For the peak-aged Al-5Cu-0.8Mg-0.15Zr-0.2Sc(-0.5Ag) alloys, it is obvious that the relationships between the amplitudes of the plastic and elastic strains, as well as the reversals to failure, are roughly linear, where the

linear correlation coefficients are ranged from −0.939 to −0.994 and can be explained by Equations (1) and (2), respectively. The values of strain fatigue parameters such as the fatigue ductility coefficient ε'_f, fatigue ductility exponent c, fatigue strength coefficient σ'_f, and fatigue strength exponent b can be determined using the data in Figure 4a–d and are listed in Tables 1 and 2 for the peak-aged Al-5Cu-0.8Mg-0.15Zr-0.2Sc(-0.5Ag) alloys subjected to low-cycle fatigue at room temperature and 200 °C. The addition of 0.5% Ag has a significant effect on the strain fatigue parameters of the Al-5Cu-0.8Mg-0.15Zr-0.2Sc at both room temperature and 200 °C, as shown in Tables 1 and 2. According to Table 1, when low-cycle fatigue deformation is performed at room temperature, the ε'_f and σ'_f values of peak-aged Al-5Cu-0.8Mg-0.15Zr-0.2Sc-0.5Ag alloy are significantly higher than those of peak-aged Al-5Cu-0.8Mg-0.15Zr-0.2Sc alloy, while the b and c values are significantly lower than those of the Al-5Cu-0.8Mg-0.15Zr-0.2Sc-0.5Ag alloy. As shown in Table 2, at the testing temperature of 200 °C, the values of the Al-5Cu-0.8Mg-0.15Zr-0.2Sc-0.5Ag alloy are significantly higher than that of the Al-5Cu-0.8Mg-0.15Zr-0.2Sc alloy, while the b and c values of peak-aged Al-5Cu-0.8Mg-0.15Zr-0.2Sc-0.5Ag alloy are lower than those of peak-aged Al-5Cu-0.8Mg-0.15Zr-0.2Sc alloy.

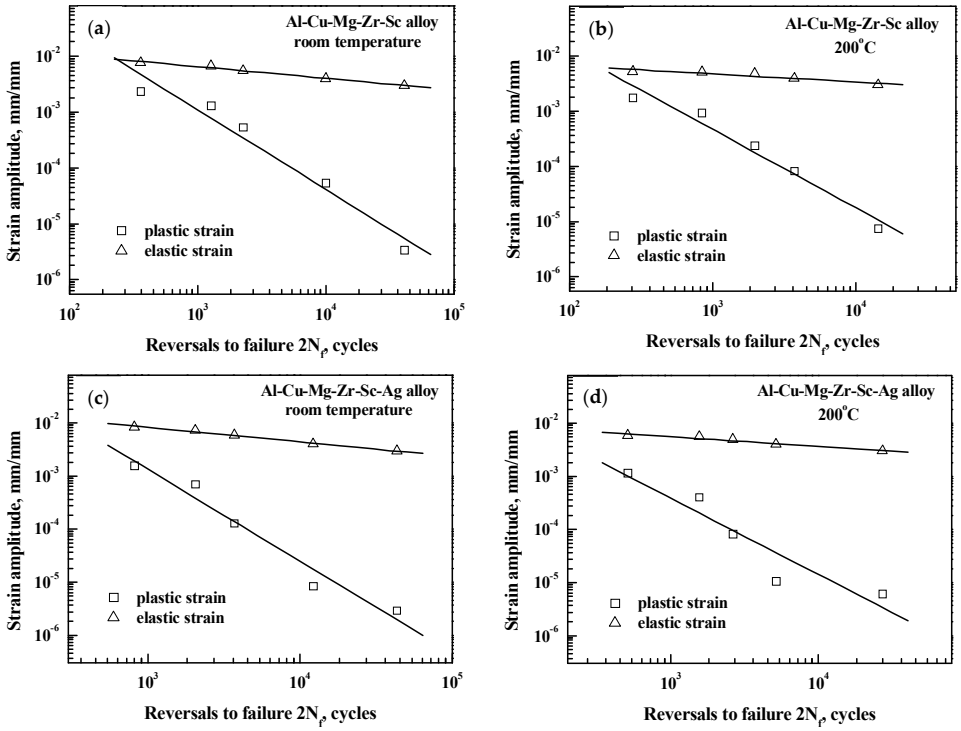

Figure 4. Plastic and elastic strain amplitudes versus reversals in failure curves of peak-aged Al-5Cu-0.8Mg-0.15Zr-0.2Sc alloy at different testing temperatures: (**a**) room temperature, (**b**) 200 °C, and Al-5Cu-0.8Mg-0.15Zr-0.2Sc-0.5Ag alloy at different testing temperatures: (**c**) room temperature, (**d**) 200 °C.

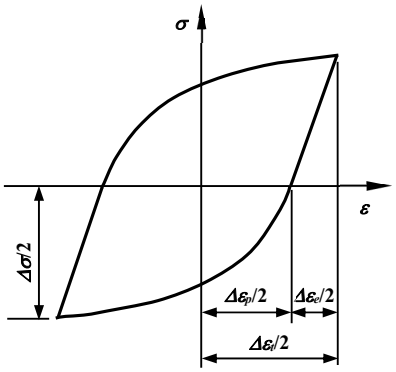

Figure 5. Schematic half-life hysteresis loop.

Table 1. Strain fatigue parameters of peak-aged Al-5Cu-0.8Mg-0.15Zr-0.2Sc(-0.5Ag) alloys at RT.

Alloy	ft (%)	c	σ'_f (MPa)	b	K' (MPa)	n'
Al-5Cu-0.8Mg-0.15Zr-0.2Sc	20.89	−1.426	1985.9	−0.209	709.5	0.084
Al-5Cu-0.8Mg-0.15Zr-0.2Sc-0.5Ag	29.43	−1.732	3994.2	−0.276	706.2	0.066

Table 2. Strain fatigue parameters of peak-aged Al-5Cu-0.8Mg-0.15Zr-0.2Sc(-0.5Ag) alloys at 200 °C.

Alloy	ε'_f (%)	c	σ'_f (MPa)	b	K' (MPa)	n'
Al-5Cu-0.8Mg-0.15Zr-0.2Sc	8.59	−1.421	822.5	−0.147	740.3	0.099
Al-5Cu-0.8Mg-0.15Zr-0.2Sc-0.5Ag	7.92	−1.437	1229.3	−0.181	939.8	0.108

3.3. Cyclic Stress–Strain Behavior

The cyclic stress–strain behavior, which may be explained by the cyclic stress amplitude versus plastic strain amplitude curve, depicts the actual stress-strain properties of the materials under the low-cycle fatigue loading situation. For the peak-aged Al-5Cu-0.8Mg-0.15Zr-0.2Sc(-0.5Ag) alloys at both room temperature and 200 °C, Figure 6a,b show the cyclic stress amplitude against plastic strain amplitude curves. The cyclic stress amplitude and plastic strain amplitude were determined from the half-life hysteresis loops. It can be seen that the peak-aged Al-5Cu-0.8Mg-0.15Zr-0.2Sc(-0.5Ag) alloys subjected to the low-cycle fatigue deformation exhibit a linear relationship between the cyclic stress amplitude and plastic strain amplitude. This relationship exists at both room temperature and 200 °C. Absolutely, a power law can be used to describe the relationship between the amplitude of the cyclic stress and the amplitude of the plastic strain, that is,

$$\Delta\sigma/2 = K'(\Delta\varepsilon_p/2)^{n'} \quad (3)$$

where $\Delta\sigma/2$ is the cyclic stress amplitude, K' is the cyclic strength coefficient, and n' is the cyclic strain hardening exponent. According to the data in Figure 6 and a linear regression analysis, the typical values of strain fatigue parameters such as the cyclic strength coefficient K' and the cyclic strain hardening exponent n' for peak-aged Al-5Cu-0.8Mg-0.15Zr-0.2Sc(-0.5Ag) alloys subjected to low-cycle fatigue at room temperature and 200 °C are listed in Tables 1 and 2. Under the room temperature low-cycle fatigue condition, the addition of 0.5% Ag reduces the n' value but has no effect on the K' value for the peak-aged Al-5Cu-0.8Mg-0.15Zr-0.2Sc alloy. When the low-cycle fatigue deformation is performed at 200 °C, the addition of 0.5% Ag increases both K' and n' values of the peak-aged Al-5Cu-0.8Mg-0.15Zr-0.2Sc alloy.

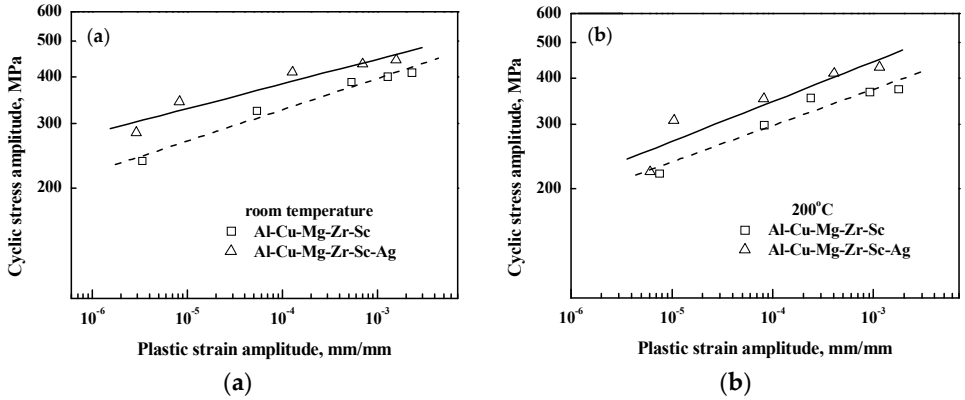

Figure 6. Cyclic stress amplitude versus plastic strain amplitude curves for peak-aged Al-5Cu-0.8Mg-0.15Zr-0.2Sc(-0.5Ag) alloys at different testing temperatures: (**a**) room temperature, (**b**) 200 °C.

3.4. Fatigue Crack Initiation and Propagation

Figure 7 depicts the morphologies of the fatigue crack initiating region for peak-aged Al-5Cu-0.8Mg-0.15Zr-0.2Sc(-0.5Ag) alloys at various testing temperatures and total strain amplitudes. The arrow points to the origin of fatigue crack. From Figure 7a–d, it is clear that for the peak-aged Al-5Cu-0.8Mg-0.15Zr-0.2Sc alloy with and without the Ag element, the morphologies of the fatigue crack initiating regions at the same total strain amplitude are very similar. The fatigue crack also begins trans granularly at the free surface of the fatigue specimen whether the testing temperature is at room temperature or 200 °C. This indicates that at the same testing temperature, the addition of Ag has little impact on the initiating mode of low-cycle fatigue cracks.

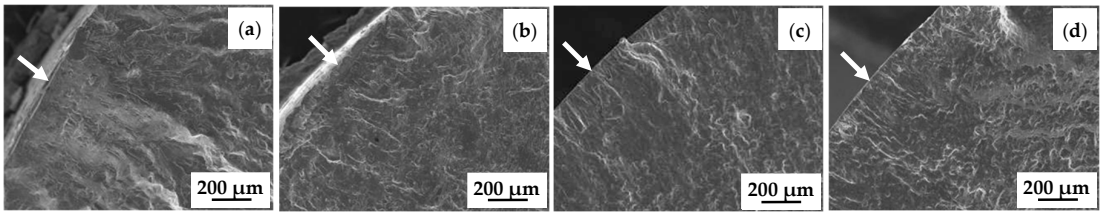

Figure 7. Morphologies of fatigue crack initiating region at different temperatures and total strain amplitudes for peak-aged Al-5Cu-0.8Mg-0.15Zr-0.2Sc(-0.5Ag) alloys: (**a**) RT, $\Delta\varepsilon_t/2$ = 0.4%, without Ag; (**b**) RT, $\Delta\varepsilon_t/2$ = 0.4%, with Ag; (**c**) 200 °C, $\Delta\varepsilon_t/2$ = 0.6%, without Ag; (**d**) 200 °C, $\Delta\varepsilon_t/2$ = 0.6%, with Ag.

Figure 8 depicts the morphologies of the fatigue crack propagating region for peak-aged Al-5Cu-0.8Mg-0.15Zr-0.2Sc(-0.5Ag) alloys at various testing temperatures and total strain amplitudes. The peak-aged Al-5Cu-0.8Mg-0.15Zr-0.2Sc(-0.5Ag) alloys subjected to the low-cycle fatigue deformation under different total strain amplitude at room temperature and 200 °C can be clearly seen to have a significant amount of fatigue striations in the region of the fatigue crack propagation of fatigue fracture surfaces, as shown in Figure 8a–d. It implied that the fatigue crack propagating mode under the low-cycle fatigue loading condition used in this study is trans granular for peak-aged Al-5Cu-0.8Mg-0.15Zr-0.2Sc alloys with and without the 0.5% Ag element. The presence of Ag in the peak-aged Al-5Cu-0.8Mg-0.15Zr-0.2Sc alloy has no effect on the propagating mechanism of the low-cycle fatigue crack.

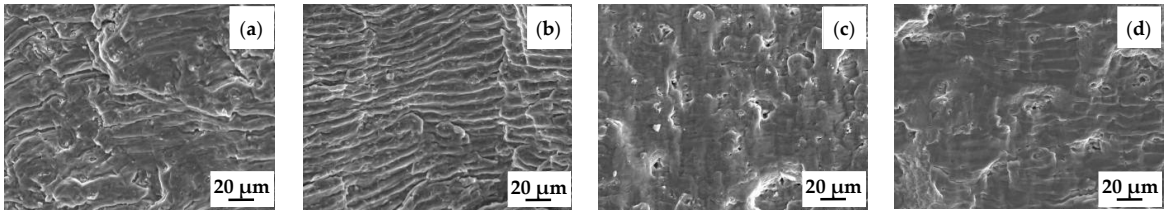

Figure 8. Morphologies of fatigue crack propagating region at different temperatures and total strain amplitudes for peak-aged Al-5Cu-0.8Mg-0.15Zr-0.2Sc(-0.5Ag) alloys: (**a**) RT, $\Delta\varepsilon_t/2$ = 0.8%, without Ag; (**b**) RT, $\Delta\varepsilon_t/2$ = 0.8%, with Ag; (**c**) 200 °C, $\Delta\varepsilon_t/2$ = 0.6%, without Ag; (**d**) 200 °C, $\Delta\varepsilon_t/2$ = 0.6%, with Ag.

4. Discussion

In general, during the low-cycle fatigue deformation controlled by the imposed total strain amplitude, such cyclic stress response behavior as the cyclic hardening, cyclic softening, and cyclic stability can be seen. The interaction between dislocations and between dislocation and precipitate is primarily responsible for the cyclic hardening. The alloys will produce a significant number of dislocations during the low-cycle fatigue deformation, and this high density of dislocations will interact with one another. Then, dislocation configurations such as the dislocation tangle and Lomer–Cottrell dislocation lock emerge, which act as effective impediments to dislocation movement. When gliding dislocations collide with precipitate particles, the dislocations either bypass the precipitate particles or pile up in front of the precipitate particles, causing local strengthening on the dislocation slip plane and thus obstructing dislocation slip. Obviously, the interaction between dislocations and between dislocations and precipitates can significantly impede dislocation movement, necessitating an increase in external load to maintain the constant strain during fatigue deformation. As a result, the cyclic stress amplitude increases, resulting in cyclic hardening. Furthermore, the blocking action of grain boundaries as dislocation slip obstacles causes a pile-up of dislocations in front of these obstacles, which is also an important element in the occurrence of cyclic hardening. The annihilation or configuration reconstruction of dislocations, which is truly equivalent to the process of dislocation recovery, is frequently the cause of cyclic softening. Dissimilar dislocations can oppose each other during movement, resulting in a decrease in slip resistance of dislocations during fatigue deformation. As a result, the induced stress required for dislocation slip decreases, resulting in the so-called softening effect. On the other hand, dislocation substructures with complicated configurations might undergo rebuilding during fatigue deformation, resulting in the creation of new dislocation topologies with substantially lower fatigue resistance. Obviously, the cyclic stress amplitude required for additional dislocation slip decreases, resulting in a softening effect. The following procedure can be used to rearrange dislocations. During tensile deformation, moveable dislocations can evade the accumulation in front of them by climbing or cross-sliding around precipitate particles. Interaction between dislocations occurs at these precipitate particles during reverse compressive deformation. Some dislocations must depart their initial sliding plane, resulting in the formation of a plastic zone. During fatigue deformation, the preceding process is continually repeated, and these plastic zones join to form an evenly distributed dislocation substructure in a three-dimensional space. In fact, cyclic hardening and cyclic softening are two conflicting processes during low-cycle fatigue loading. The material exhibits cyclic hardening if the cyclic hardening effect is greater than the cyclic softening effect. If the cyclic hardening effect is less than the cyclic softening effect, the material exhibits cyclic softening. The hardening effect and softening effect cancel out when the cyclic effects of hardening and softening reach equilibrium, and the material then displays a stable cyclic stress response behavior [24].

As previously mentioned, the addition of Ag improves the cyclic deformation resistance of peak-aged Al-5Cu-0.8Mg-0.15Zr-0.2Sc alloy at both room temperature and 200 °C. It has been well documented [25–27] that the addition of Ag element can lead to a large increase in the number of precipitates in the aged alloy, and the precipitates in the Ag

containing Al-Cu-Mg series alloys are primarily in the Ω phase with higher thermal stability than in the other phase. The TEM images at the fracture surface for the peak-aged Al-5.3Cu-0.8Mg-0.15Zr-0.2Sc(-0.5Ag) alloys following low-cycle fatigue fracture are shown in Figure 9. At room temperature or 200 °C, the dislocation density in the Al-5Cu-0.8Mg-0.15Zr-0.2Sc-0.5Ag alloy is substantially more than that in the Al-5Cu-0.8Mg-0.15Zr-0.2Sc alloy following fatigue failure at the same total strain amplitude, as shown in Figure 9a–d. It means that the strengthening effect is relatively stronger due to the formation of phase in the peak-aged Al-5Cu-0.8Mg-0.15Zr-0.2Sc-0.5Ag alloy. The aforementioned factor will provide a greater impediment to dislocation movement, resulting in the occurrence of tensile and compressive plastic deformation corresponding to each cycle at the higher applied stress to maintain the constant strain. As a result, when low-cycle fatigue deformation is performed at the same total strain amplitude, the Al-5Cu-0.8Mg-0.15Zr-0.2Sc-0.5Ag alloy demonstrates more cyclic deformation resistance than the Al-5Cu-0.8Mg-0.15Zr-0.2Sc alloy. Actually, the higher the cyclic deformation resistance during low-cycle fatigue loading, the stronger the alloy's resistance to fatigue damage, and thus the peak-aged Al-5Cu-0.8Mg-0.15Zr-0.2Sc-0.5Ag alloy has a longer fatigue life than the peak-aged Al-5Cu-0.8Mg-0.15Zr -0.2Sc alloy.

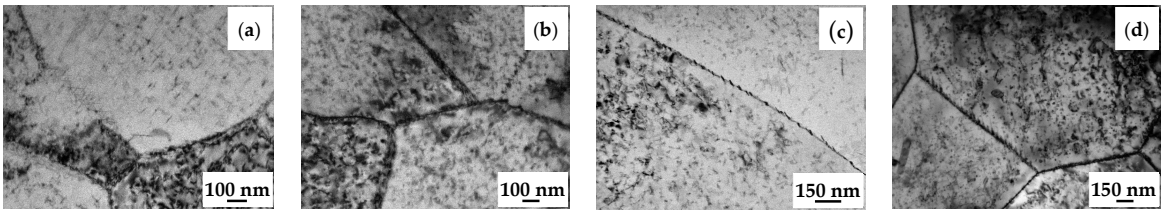

Figure 9. TEM images for peak-aged Al-5.3Cu-0.8Mg-0.15Zr-0.2Sc(-0.5Ag) alloys after low-cycle fatigue fracture at different testing temperatures and imposed total strain amplitudes: (**a**) RT, $\Delta\varepsilon_t/2$ = 0.8%, without Ag; (**b**) RT, $\Delta\varepsilon_t/2$ = 0.8%, with Ag; (**c**) 200 °C, $\Delta\varepsilon_t/2$ = 0.6%, without Ag; (**d**) 200 °C, $\Delta\varepsilon_t/2$ = 0.6%, with Ag.

5. Conclusions

(1) The peak-aged Al-5Cu-0.8Mg-0.15Zr-0.2Sc alloy exhibits cyclic hardening followed by cyclic stability or cyclic hardening during low-cycle fatigue deformation at room temperature and different total strain amplitudes, whereas the peak-aged Al-5Cu-0.8Mg-0.15Zr-0.2Sc-0.5Ag alloy exhibits cyclic hardening followed by cyclic stability or cyclic hardening.

(2) The peak-aged Al-5Cu-0.8Mg-0.15Zr-0.2Sc-0.2Sc-0.5Ag alloy exhibits the cyclic stability or the cyclic hardening during the low-cycle fatigue deformation at 200 °C and different total strain amplitudes, in contrast to the peak-aged Al-5Cu-0.8Mg-0.15Zr-0.2Sc-0.2Sc alloy.

(3) The peak-aged Al-5Cu-0.8Mg-0.15Zr-0.2Sc-0.5Ag alloy has a stronger cyclic deformation resistance than the peak-aged Al-5Cu-0.8Mg-0.15Zr-0.2Sc alloy at temperatures of both room temperature and 200 °C. The low-cycle fatigue life is significantly increased with the addition of 0.5% Ag.

(4) Fatigue cracks begin and spread trans granularly for peak-aged Al-5Cu-0.8Mg-0.15Zr-0.2Sc(-0.5Ag) alloys exposed to low-cycle fatigue deformation at room temperature and 200 °C. The 0.5% Ag addition has no effect on the low-cycle fatigue crack's beginning or propagating mode.

Author Contributions: Conceptualization, Y.W. and L.C.; methodology, Y.W.; software, Y.W.; validation, Y.W., L.C. and G.Z.; formal analysis, G.Z.; investigation, R.L.; resources, G.Z.; data curation, Y.W.; writing—original draft preparation, Y.W.; writing—review and editing, L.C.; visualization, R.L.; supervision, S.Z.; project administration, L.C.; funding acquisition, S.Z. All authors have read and agreed to the published version of the manuscript.

Funding: This research was funded by Shenyang University of Technology, grant number [2022JH2/101300078] and the APC was funded by [zhouge@sut.edu.cn].

Data Availability Statement: No new data were created or analyzed in this study. Data sharing is not applicable to this article.

Conflicts of Interest: The authors declare no conflict of interest.

References

1. Jiang, F.; Wen, K.; Jian, H.-G.; Jiang, C.-L.; Zhao, J.; Jiang, L. Existing form and action mechanism of minor scandium and zirconium in Al-Cu-Mg alloy. *J. Cent. South Univ.* **2010**, *17*, 19–23. [CrossRef]
2. Cavaliere, P. Effect of minor Sc and Zr addition on the mechanical properties of friction stir processed 2024 aluminium alloy. *J. Mater. Sci.* **2006**, *41*, 4299–4302. [CrossRef]
3. Yu, K.; Li, W.; Li, S.; Zhao, J. Mechanical properties and microstructure of aluminum alloy 2618 with Al3(Sc. Zr) phases. *Mater. Sci. Eng. A* **2004**, *368*, 88–93. [CrossRef]
4. Xiao, D.H.; Song, M.; Huang, B.Y.; Yi, J.H.; He, Y.H.; Li, Y.M. Effect of Sc addition on microstructure and mechanical properties of Al-Cu-Mg-Ag-Zr alloy. *Mater. Sci. Technol.* **2009**, *25*, 747–752. [CrossRef]
5. Fan, J.C.; Yang, B.W.; Wang, Y.; Gao, M.; Guan, R. Enhancing the tensile strength and heat resistance induced by high-density ω phases in an Al-Cu-Mg-Ag alloy. *J. Mater. Res. Technol.* **2022**, *18*, 3347–3357. [CrossRef]
6. Al-Obaisi, A.M.; El-Danaf, E.A.; Ragab, A.E.; Soliman, M.S. Precipitation hardening and statistical modeling of the aging parameters and alloy compositions in Al-Cu-Mg-Ag alloys. *J. Mater. Eng. Perform.* **2016**, *25*, 2432–2444. [CrossRef]
7. Liu, X.Y.; Pan, Q.L.; Zheng, L.Y.; Fu, Q.R.; Gao, F.; Li, M.X.; Bai, Y.M. Effect of aging temper on the thermal stability of Al-Cu-Mg-Ag heat-resistant alloy. *Mater. Design* **2013**, *46*, 360–365. [CrossRef]
8. Gu, Y.; Liu, Z.; Yu, D.; Liu, B.; Lin, M.; Zeng, S. Growth of Ω plates and its effect on mechanical properties in Al-Cu-Mg-Ag alloy with high content of silver. *J. Mater. Eng. Perform.* **2013**, *22*, 1708–1715. [CrossRef]
9. Yu, Z.; Li, H.; Cai, P.; Fu, X.; Feng, Z.; Zhang, L.; Wang, J.; Xiao, N. Effect of aging route on the precipitation behavior and thermal stability of Al-Cu-Mg-Ag alloy. *J. Mater. Res. Technol.* **2023**, *23*, 2010–2019. [CrossRef]
10. Song, M.; Chen, K.H.; Huang, L.P. Effects of Ag addition on mechanical properties and microstructures of Al-8Cu-0.5Mg alloy. *Trans. Nonferrous Met. Soc.* **2006**, *16*, 766–771. [CrossRef]
11. Zhou, X.; Liu, Z.; Bai, S.; Liu, M.; Ying, P. The influence of various Ag additions on the nucleation and thermal stability of Ω phase in Al-Cu-Mg alloys. *Mat. Sci. Eng. A* **2013**, *564*, 186–191. [CrossRef]
12. Ma, F.Y.; Liu, Z.Y.; Hou, Y.H.; Xia, Q.K.; Bai, S.; Luo, H. Effect of Ag content on evaluated-temperature mechanical properties and thermal stability of Al-Cu-Mg-Ag alloys. *Rare Metal Mat. Eng.* **2010**, *39*, 482–485.
13. Wang, J.; Xie, J.; Mao, Z.; Liang, T.; Wang, A.; Wang, W.; Hao, S. Microstructure evolution and mechanical properties of the Al-Cu-Mg-Ag alloy during non-isothermal aging. *J. Alloy Compd.* **2023**, *942*, 169031. [CrossRef]
14. Gazizov, M.; Kaibyshev, R. Low-cyclic fatigue behaviour of an Al-Cu-Mg-Ag alloy under T6 and T840 conditions. *J. Mater. Sci. Technol.* **2017**, *33*, 688–698. [CrossRef]
15. Gazizov, M.; Kaibyshev, R. High cyclic fatigue performance of Al-Cu-Mg-Ag alloy under T6 and T840 conditions. *Trans. Nonferrous Met. Soc.* **2017**, *27*, 1215–1223. [CrossRef]
16. Wang, J.; Liu, Z.; Bai, S.; Cao, J.; Zhao, J.; Zeng, D. Microstructure and three-point bending fatigue behavior of Al-Cu-Mg-Ag alloys with various Mg contents. *J. Mater. Eng. Perform.* **2019**, *28*, 6614–6625. [CrossRef]
17. Burba, M.E.; Caton, M.J.; Jha, S.K.; Szczepanski, C.J. Effect of aging treatment on fatigue behavior of an Al-Cu-Mg-Ag alloy. *Metall. Mater. Trans.* **2013**, *44*, 4954–4967. [CrossRef]
18. Bai, S.; Liu, Z.; Gu, Y.; Zhou, X.; Zeng, S. Microstructures and fatigue fracture behavior of an Al-Cu-Mg-Ag alloy with a low Cu/Mg ratio. *Mat. Sci. Eng. A* **2011**, *530*, 473–480. [CrossRef]
19. Lin, G.; Zhang, H.W.; Li, H.Z.; Guan, L.N.; Huang, L.J. Effect of Mg content on microstructure and mechanical properties of Al-Cu-Mg-Ag alloys. *Rare Metal Mater. Eng.* **2010**, *39*, 52–55.
20. Zhemchuzhnikova, D.A.; Gazizov, M.R.; Kaibyshev, R.O. Crack resistance of an alloy of the Al-Cu-Mg-Ag system. *Met. Sci. Heat Treat.* **2017**, *59*, 498–503. [CrossRef]
21. Bai, S.; Liu, Z.; Li, Y.; Hou, Y.; Chen, X. Microstructures and fatigue fracture behavior of an Al-Cu-Mg-Ag alloy with addition of rare earth Er. *Mater. Sci. Eng. A* **2010**, *527*, 1806–1814. [CrossRef]
22. Lumley, R.N.; O'Donnell, R.G.; Polmear, I.J.; Griffiths, J.R. Enhanced fatigue resistance by underageing an Al-Cu-Mg-Ag alloy. *Mater. Forum* **2005**, *29*, 256–261.
23. Hu, Y.; Liu, Z.; Zhao, Q.; Bai, S.; Liu, F. P-texture effect on the fatigue cack propagation resistance in an Al-Cu-Mg alloy bearing a small amount of silver. *Materials* **2018**, *11*, 2481. [CrossRef] [PubMed]
24. Chen, L.J.; Wang, X.; Ma, C.Y.; Che, X. Low cycle fatigue behaviour of hot extruded Al-4Mg-1Nd alloy. *Mater. Sci. Technol.* **2010**, *26*, 604–609. [CrossRef]
25. Ringer, S.P.; Hono, K. NucIeation of precipitates in aged Al-Cu-Mg-(Ag) alloys with high Cu:Mg ratios. *Acta Mater.* **1996**, *44*, 1883–1898. [CrossRef]

26. Bai, S.; Ying, P.; Liu, Z.; Wang, J.; Li, J. Quantitative transmission electron microscopy and atom probe tomography study of Ag-dependent precipitation of Ω phase in Al-Cu-Mg alloys. *Mater. Sci. Eng. A* **2017**, *687*, 8–16. [CrossRef]
27. Ying, P.; Lin, C.; Liu, Z.; Bai, S.; Levchenko, V.; Zhang, P.; Wu, J.; Yang, T.; Huang, M.; Yang, G.; et al. Pre-aging effect on the formation of Ω phase and mechanical properties of the Al-Cu-Mg-Ag alloy. *Metals* **2022**, *12*, 1208. [CrossRef]